molecular pharmaceutics

pubs.acs.org/molecularpharmaceutics

Article

Pharmacokinetic Modeling of [^{18}F]MC225 for Quantification of the P-Glycoprotein Function at the Blood–Brain Barrier in Non-Human Primates with PET

Lara García-Varela, Wejdan M. Arif, David Vállez García, Takeharu Kakiuchi, Hiroyuki Ohba, Norihiro Harada, Tetsuro Tago, Philip H. Elsinga, Hideo Tsukada, Nicola Antonio Colabufo, Rudi A. J. O. Dierckx, Aren van Waarde, Jun Toyohara, Ronald Boellaard, and Gert Luurtsema*

Cite This: *Mol. Pharmaceutics* 2020, 17, 3477–3486

Read Online

ACCESS | Metrics & More | Article Recommendations | Supporting Information

ABSTRACT: [^{18}F]MC225 has been developed as a weak substrate of P-glycoprotein (P-gp) aimed to measure changes in the P-gp function at the blood–brain barrier with positron emission tomography. This study evaluates [^{18}F]MC225 kinetics in non-human primates and investigates the effect of both scan duration and P-gp inhibition. Three rhesus monkeys underwent two 91-min dynamic scans with blood sampling at baseline and after P-gp inhibition (8 mg/kg tariquidar). Data were analyzed using the 1-tissue compartment model (1-TCM) and 2-tissue compartment model (2-TCM) fits using metabolite-corrected plasma as the input function and for various scan durations (10, 20, 30, 60, and 91 min). The preferred model was chosen according to the Akaike information criterion and the standard errors (%) of the estimated parameters. For the 91-min scan duration, the influx constant K_1 increased by 40.7% and the volume of distribution (V_T) by 30.4% after P-gp inhibition, while the efflux constant k_2 did not change significantly. Similar changes were found for all evaluated scan durations. K_1 did not depend on scan duration (10 min—K_1 = 0.2191 vs 91 min—K_1 = 0.2258), while V_T and k_2 did. A scan duration of 10 min seems sufficient to properly evaluate the P-gp function using K_1 obtained with 1-TCM. For the 91-min scan, V_T and K_1 can be estimated with a 2-TCM, and both parameters can be used to assess P-gp function.

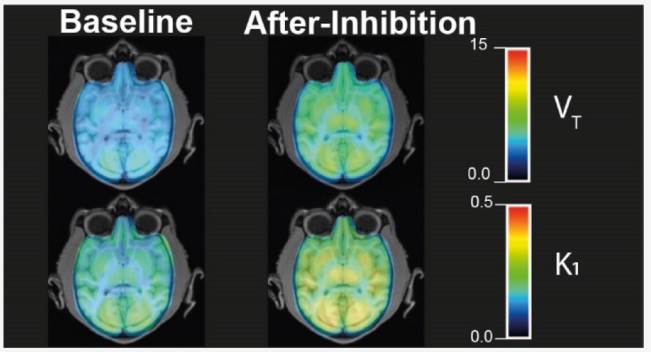

KEYWORDS: *kinetic evaluation, PET, P-gp inhibition, P-gp tracer, rhesus macaque*

1. INTRODUCTION

The blood–brain barrier (BBB) is a physical membrane that separates the blood from the brain and is mainly composed of three cellular elements: endothelial cells, astrocytes end-feet, and pericytes.[1,2] The cerebral endothelial cells connected by tight junctions impede the paracellular diffusion of hydrophilic compounds.[1,3] Moreover, the BBB also expresses multiple influx and efflux transporters, which regulate the transport of exogenous and endogenous substances.[4] Thereby, BBB's main purpose is to protect the central nervous system (CNS) and ensure a controlled and stable environment for the correct neural function.[4,5]

Members of the ATP-binding cassette (ABC) family are considered the most important efflux transporters at the BBB. Their main function is to protect the brain from harmful substances. P-Glycoprotein (P-gp) is the best known ABC transporter,[4] and a wide variety of compounds have been identified as P-gp substrates or P-gp modulators. Therefore, P-gp is involved in various drug–drug interactions (DDIs) at the BBB. P-gp substrates are compounds that are transported by P-gp from the brain to the blood. P-gp modulators are compounds that can modify the P-gp function or expression. For instance, P-gp inhibitors increase the P-gp function by blocking the ligand-binding site of the P-gp transporters or by preventing the ATP hydrolysis. P-gp inducers increase P-gp expression by the activation of transcription factors such as the pregnane xenobiotic receptor.[6−8] Increases of P-gp function can reduce the concentration of drugs inside the brain and therefore lead to decreased drug efficacy.[8,9] On the other hand, decreases in P-gp function can cause increased concentrations of neurotoxic compounds inside the CNS and thus have been related to the onset of several neurodegenerative diseases.[10−12]

Received: May 11, 2020
Revised: August 5, 2020
Accepted: August 5, 2020
Published: August 5, 2020

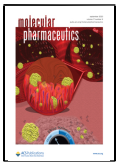

https://dx.doi.org/10.1021/acs.molpharmaceut.0c00514
Mol. Pharmaceutics 2020, 17, 3477–3486

Positron emission tomography (PET) with specific P-gp tracers is a suitable technique to measure the P-gp transporter function in vivo.[13] Savolainen et al. (2017) introduced a fluorine-18-labeled tracer, called [^{18}F]MC225, which proved to be selectively transported by P-gp and not by BCRP, another important ABC transporter at the BBB.[14] According to preclinical studies performed in mice and rats, this novel tracer behaves as a weak P-gp substrate. This results in the higher brain uptake of [^{18}F]MC225 at the baseline (V_T = 6.6−11) compared with the widely used P-gp tracer (*R*)-[^{11}C]verapamil (V_T = 1.1−2.3).[14−16] This elevated baseline uptake would allow measuring increases of P-gp function as may occur in patients with drug-resistant epilepsy[17] and also decreases of P-gp function in neurodegenerative diseases.[18,19]

Based on a kinetic evaluation of [^{18}F]MC225 in rats, the 1-tissue compartment model (1-TCM) was selected as the model of choice for quantification of [^{18}F]MC225 transport across the BBB. This evaluation was performed using scans acquired at baseline and after tariquidar administration, which cause P-gp inhibition. The largest changes after P-gp-inhibition (compared to baseline) were found in the influx rate constant K_1. For this reason, and in accordance with previous publications, K_1 is considered as the most suitable parameter to estimate P-gp function at the BBB.[15,20,21]

K_1 measures the transport of the tracer from the plasma to tissue. Based on the Fick principle and Renkin−Crone model,[22,23] this parameter depends on blood flow and the unidirectional extraction fraction. Lipophilic tracers, such as [^{18}F]MC225 (log *D* = 3.0),[14] have a large extraction fraction, and therefore, K_1 is susceptible to changes in the blood flow.[24] Moreover, errors in the input function, especially immediately after the injection of the tracer (plasma peak), can also affect the accuracy of K_1 estimation. Thus, more robust parameters, models, and scanning procedures to assess the P-gp function should be investigated.

This study explores the pharmacokinetics of [^{18}F]MC225 in non-human primates (NHP), which approaches human conditions more precisely in terms of P-gp expression than rodents.[25] To this aim, [^{18}F]MC225 kinetics were assessed at baseline and after P-gp inhibition, using dynamic PET scans with arterial blood sampling. We assessed the effect of varying scan durations and P-gp inhibition on kinetic model performance. Moreover, we compared the suitability of K_1 and V_T to measure P-gp function in terms of capturing the effects of P-gp inhibition and parameter robustness at various evaluated scan durations.

2. EXPERIMENTAL SECTION

2.1. Tracer Production. The precursor 5-[3-(6,7-dimethoxy-3,4-dihydro-1*H*-isoquinolin-2-yl)-propyl]-5,6,7,8-tetrahydro-naphthalen-1-ol (MC226) and the cold reference compound, 5-(1-(2-fluoroethoxy))-[3-(6,7-dimethoxy-3,4-dihydro-1*H*-isoquinolin-2-yl)-propyl]-5,6,7,8-tetrahydronaphthalen (MC225), were supplied by the University of Bari, Italy. Tariquidar methanesulfonate hydrate was purchased from MedChemExpress (Monmouth Junction, NJ, USA). [^{18}F]MC225 was synthesized on a multipurpose synthesizer (F120, Sumitomo Heavy Industries, Tokyo, Japan) as previously described.[14,15]

2.2. Animals. The study was performed at the Central Research Laboratory, Hamamatsu Photonics (Hamamatsu, Japan) in collaboration with the Tokyo Metropolitan Institute of Gerontology (Tokyo, Japan). Three healthy-male rhesus monkeys (*Macaca mulatta*; Hamri, Ibaraki, Japan) were used. Monkeys were individually housed in the U.S. National Institute of Health (NIH) standard adapted stainless-steel cages, in a controlled room with a temperature of 24 ± 4 °C, a humidity 50 ± 20%, and under a 14 h light/10 h dark cycle. They were fed with 120 g of chow (Certified Primate Diet 5048, PMI Nutrition) in the morning and 100 g of raw sweet potato in the evening. The weight (7.26 ± 0.78 kg) and the behavior of the animals were monitored during the study. The study was carried out in accordance with the recommendations of the NIH, the guidelines of the Ethics Committee of the Central Research Laboratory, Hamamatsu Photonics (approval HPK-2016-07A), and the Institutional Animal Care and Use Committee of Tokyo Metropolitan Institute of Gerontology (approval 16067).

2.3. Data Collection. *2.3.1. Experimental Design.* All animals underwent two 91-min dynamic PET scans using [^{18}F]MC225: at baseline and after P-gp inhibition, within 1 month. P-gp inhibition consisted of intravenous (i.v.) injection of the P-gp inhibitor tariquidar[26−28] (8 mg/kg of body weight) 15 min before the PET scan. Tariquidar methanesulfonate hydrate (11 mg) was dissolved in 3 mL of saline as a suspension solution. The injection volume was adjusted to the weight of each monkey. The tariquidar methanesulfonate hydrate solution was slowly infused through a catheter inserted into the saphenous vein.

2.3.2. PET/Magnetic Resonance Imaging Data. A structural T_1 weighted magnetic resonance imaging (MRI) scan (Signa Excite HDxT 3.0T, GE Healthcare, Milwaukee, WI, USA) was made before the first PET scan. All animals underwent 91-min dynamic PET scan (SHR-38000, Hamamatsu Photonics, Shizuoka, Japan) with arterial blood sampling. Animals were anesthetized (2.5% sevoflurane) during their transport but remained awake during the scans with their head immobilized using a fixation device. The monkeys were positioned in the camera in a sitting position, with stereotactic coordinates aligned parallel to the orbito-meatal plane.

A transmission scan was performed before the acquisition of the PET data using a rotating ^{68}Ge/^{68}Ga rod source (60 min), and its information was used for attenuation and scatter correction of the PET images. Animals were injected with [^{18}F]MC225 (684 ± 64 MBq) at the start of the emission scan, via the saphenous vein over a period of 30 s as a single bolus.

PET images were reconstructed using filtered back projection with a Hanning filter of 4.5 mm and were composed of 49 frames (6 × 10, 6 × 30, 12 × 60, and 25 × 180 s).

2.3.3. Blood Data. After the administration of the tracer, 19 blood samples (0.5 mL) were drawn from a cannula placed in the posterior tibial artery (at 8, 16, 24, 32, 40, 48, 56, and 64 s and 1.5, 2.5, 4, 6, 10, 20, 30, 45, 60, 75, and 91 min). Then, plasma and blood were separated by centrifugation (12,000 rpm, 60 s), and the radioactivity was measured using a gamma counter (1480 Wizard, PerkinElmer, Waltham, MA, USA).

Parent fraction and radioactive metabolites of [^{18}F]MC225 were analyzed following tracer injection (16, 40, and 64 s and 6, 10, 30, 45, 60, 75, and 91 min). Ethanol was added to the plasma fraction to precipitate the plasma proteins. The supernatant of these samples was analyzed using thin-layer chromatography plates (silica gel 60 F254, Merck, Millipore, Burlington, MA, USA) with a mobile phase of methanol/ethyl acetate (1/9). The parent [retention factor (R_f) = 0.4] and

https://dx.doi.org/10.1021/acs.molpharmaceut.0c00514
Mol. Pharmaceutics 2020, 17, 3477−3486

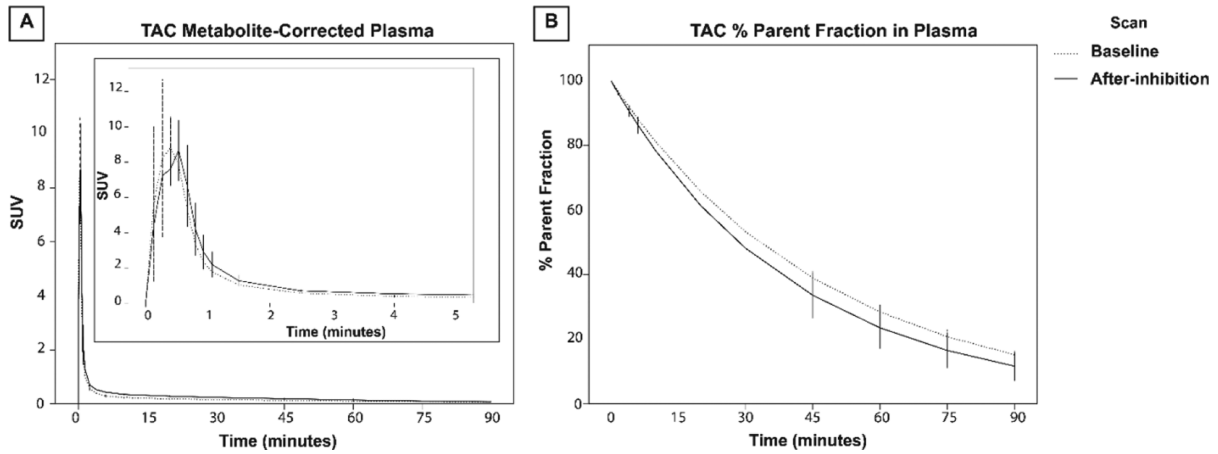

Figure 1. Mean ± SD metabolite-corrected plasma TAC (A) and percentage of parent [^{18}F]MC225 (B) at baseline and after-inhibition scans.

metabolized fractions ($R_f = 0$) were assessed using a phosphor imaging plate and a bioimaging analyzer (FLA-7000, Fuji Film, Tokyo, Japan).

The percentage of the metabolites in plasma was calculated for each subject by fitting a single exponential equation to the values obtained from the metabolite analysis, using an iterative nonlinear least squares approach using GraphPad software (GraphPad Prism version 7.02, CA, USA): $Y = (Y_0 - \text{plateau}) \times \exp(-K_e \times X) + \text{plateau}$,[29] where Y is the percentage of parent fraction at different time points, Y_0 is the intercept, which was fixed to 100% (percentage of parent fraction at the beginning of the scan), K_e is the first-order elimination constant, and X is the time.

2.4. Data Analysis. *2.4.1. Input Function.* The radioactivity measured in blood samples was corrected for decay from the time of tracer administration, and time−activity curves (TAC) of whole-blood and plasma were calculated using standardized uptake values: SUV = radioactive concentration at time (T) (kBq/mL)/[injected dose (MBq)/body weight (kg)]. The metabolite-corrected plasma TAC was calculated using SUV from plasma samples multiplied by the percentage of parent fraction, as described above.

A semilogarithmic plot of the tracer concentration in plasma, corrected for metabolites, versus time was performed to assess the compartmental model for plasma kinetics. The tracer elimination from the plasma was described with a one-compartment model. Therefore, the rate constant of elimination (K_e) and the biological half-life ($T_{1/2}$) were calculated by fitting a single exponential curve, $Y = Y_0 \times \exp(-K_e \times X)$, to the metabolite-corrected plasma TAC of each subject, by an iterative nonlinear least squares approach using GraphPad software, where Y is the SUV value in plasma-corrected for metabolites; Y_0 is the intercept; K_e is the first-order elimination constant, and X is the time. Y_0 was fixed to the concentration values at 32 s after tracer injection (plasma peak). The half-life of the tracer was calculated as $T_{1/2} = \ln(2)/K_e$.[30]

2.4.2. Positron Emission Tomography/Magnetic Resonance Imaging. Images were processed using PMOD v3.8 software (PMOD Technologies, Zürich, Switzerland). All scans were registered to a reference MRI template defined in the Montreal Neurological Institute (MNI) monkey space.[31−33] The individual MRI was registered to the reference MRI using a three-probability map normalization.[33,34] Then, [^{18}F]MC225 PET images were aligned to their corresponding MRI by rigid transformation, using a summation of all frames (Supporting Information). Head motion correction was not applied to the data.

Several volumes-of-interests (VOIs) were selected from a brain atlas:[32] basal ganglia, brainstem, cerebellum, cingulate cortex, hippocampus, hypothalamus, insular cortex, midbrain, occipital cortex, orbito-frontal cortex, parietal cortex, striatum, temporal cortex, thalamus, and white matter. Additionally, a VOI covering the whole brain was included.

2.4.3. Pharmacokinetic Analysis. Metabolite-corrected plasma and whole-blood TACs were used as the input function to perform pharmacokinetic modeling using PMOD v3.8 software.

During pharmacokinetic analyses, blood delay was first corrected by estimating the delay of the whole brain TAC and then fixing that value for the rest of the regions. Different plasma input compartment model fits were evaluated, including 1-TCM, 2-tissue compartment model (2-TCM), and irreversible 2-TCM ($k_4 = 0$) with scan durations of 10, 20, 30, 60, and 91 min. The effect of fractional volume of blood (v_B) for each model was explored by either fixing the value to 3, 4, 5, 6, and 7% or used as a fit parameter. The selection of the most appropriate model for each scan duration was based on the Akaike information criterion (AIC) and the standard errors (SE %) of the estimated parameters. Finally, changes in the pharmacokinetic parameters of each kinetic model between baseline and after-inhibition scans were also explored for all scan durations.

During the pharmacokinetic modeling, no constraints were applied to the fit parameters. However, these parameters with SE % higher than 1000% were considered unreliable and excluded for further analysis.

2.4.4. Parametric Images. Parametric images were calculated using a basis function implementation of the 2-TCM for illustrative purposes only (Figure 5). The metabolite-corrected plasma TAC was used as the input function for 2-TCM (v_B = 6%), using PMOD. Parametric images were made for one subject using 91-min scan durations and the baseline and after P-gp inhibition scans.

2.5. Statistical Analysis. Descriptive data are presented as mean ± standard deviation (SD), and results of the statistical analysis are shown as estimated marginal mean (EMM) ± SE. Statistical analysis was performed using IBM SPSS Statistics version 23 (IBM, Armonk, NY, USA). For each region, differences in AIC, SE %, pharmacokinetic parameters (V_T, K_1,

https://dx.doi.org/10.1021/acs.molpharmaceut.0c00514
Mol. Pharmaceutics 2020, 17, 3477−3486

k_2), and blood kinetics (K_e and $T_{1/2}$) between scans and among different scan duration were assessed by the generalized estimated equation (GEE) with the independent matrix.[35] Within the GEE, different values for fixed v_B, scan conditions, different kinetic models, and scan durations were selected as independent variables in the model. Results were considered statistically significant at $p < 0.05$, without correction for multiple comparisons. Differences in observed kinetic parameters because of P-gp inhibition were expressed as percentage change relative to the baseline values.

3. RESULTS

3.1. Tracer Production. [^{18}F]MC225 was produced with a radiochemical purity of 97.6 ± 1.0% and a molar activity higher than 36 GBq/μmol. The characteristics of the tracers are summarized in Table S1.

3.2. Input Function. At 30 min after tracer injection, the parent fraction of plasma radioactivity was 53% in baseline and 48% in after-inhibition scans. Figure 1 shows the TAC of metabolite-corrected plasma and the percentage of [^{18}F]MC225 parent tracer at baseline and after-inhibition. The statistical analysis did not find significant differences regarding the biological $T_{1/2}$ and K_e of [^{18}F]MC225 between baseline and after-inhibition scans (Table 1).

Table 1. Tracer Kinetics Calculated from the Metabolite-Corrected Plasma TAC[a]

subject	scan	K_e (s^{-1})	$T_{1/2}$ (s)
subject 1	baseline	0.015	45.73
subject 1	after-inhibition	0.013	52.84
subject 2	baseline	0.015	45.68
subject 2	after-inhibition	0.014	49.68
subject 3	baseline	0.016	42.08
subject 3	after-inhibition	0.017	40.51

[a] K_e = elimination constant, $T_{1/2}$ = biological half-life.

3.3. Plasma Input Models: Compartmental Models.

3.3.1. Blood Volume Estimation. The estimation of v_B during kinetic analysis provided values that ranged from 6 to 8%. No significant differences were found between v_B at baseline and after-inhibition (v_B baseline = 0.069 ± 0.002 and v_B after-inhibition = 0.057 ± 0.015); $p = 0.373$). When assessing the goodness of the fit, the lowest Akaike values were found with a fixed v_B of 6% (whole-brain AIC = −46 ± 3.9) and the free v_B (whole-brain AIC = −41 ± 4.9), without a statistically significant difference between both. Similarly, the lowest SE % for K_1 was found using either a fixed v_B of 6% or v_B as a free-fit parameter. K_1 values were similar for all v_B's tested. In fact, the differences in estimated K_1 when using a fixed v_B (3−7%) or free v_B were smaller than 3%. Because fixing v_B did not substantially improve the fit quality and had a minor impact on the pharmacokinetic parameters, it was decided to use v_B as a free-fit parameter for the rest of the study (more information in Table 2).

3.3.2. Model Selection for Different Scan Durations. In all evaluated scan durations, 2-TCM showed significantly lower AIC values than 1-TCM (Table S2). Differences in AIC obtained with 1-TCM and 2-TCM increased with longer scan durations. Overall, for the 10 min scans, the AIC with 1-TCM was 49% higher than the one with 2-TCM, and for the 91-min data, the AIC with 1-TCM was 146% higher than that obtained with 2-TCM. For all scan durations, the 1-TCM showed significantly lower SE % K_1 than the 2-TCM (70% lower in 10 min scan and 6% lower in 91 min). The SE % V_T was extremely high in 2-TCM for short scan durations, providing unrealistically high V_T (Table S3).

Table 2. EMM ± SE of AIC, SE % K_1, and K_1 of the Whole-Brain Region Using Different v_B

	whole-brain region		
v_B (%)	AIC	SE % K_1	K_1
3	−6.4 ± 2.27	2.33 ± 0.04	0.23 ± 0.01
4	−24.57 ± 3.42	1.77 ± 0.08	0.23 ± 0.01
5	−32 ± 7.12	1.55 ± 0.2	0.22 ± 0.01
6	−45.87 ± 3.95	1.22 ± 0.07	0.22 ± 0.01
7	−34.66 ± 6.46	1.61 ± 0.22	0.22
free	−40.92 ± 4.87	1.47 ± 0.14	0.22 ± 0.01

Estimated parameters with SE % higher than 1000% were excluded from the analysis. This occurred in 22 out of 1440 occasions and was seen for V_T and k_4 based on the 2-TCM for short-scan (10−30 min) durations and in regions such as hippocampus, brainstem, and striatum. The analysis also showed that the difference in SE % V_T between 1-TCM and 2-TCM decreased with longer scan duration, ranging from 92% difference in 10 min to 32% in 91-min scans.

Although 2-TCM showed the lowest AIC values, because of the high SE % found in the estimation of V_T and k_4, the 2-TCM was discarded as a robust model for short scans (10−30 min) but remained the model of choice for 60 and 91-min scan durations. Figure 2 shows representative 1-TCM and 2-TCM fits of the whole brain region.

3.3.3. Effect of Scan Duration on the Pharmacokinetic Parameters. Figure 3 shows K_1, V_T, and k_2 of the whole-brain region for different scan durations at baseline and after-inhibition. Based on the results above, the estimation of K_1 and V_T for each tested scan duration was performed with 1-TCM for short (<30 min) and 2-TCM for long scans (>60 min). K_1 remained relatively unaffected by varying the scan duration while for V_T, the differences among the scan durations were more pronounced with a 62% lower V_T at 10 min than at 91 min. The k_2 values varied randomly across the various tested scan durations.

3.3.4. Effect of P-gp Inhibition. Figure 4 displays the mean values of V_T, K_1, and k_2 of all regions for the three subjects at baseline and after-inhibition scans, using the 91-min scan duration. As can be observed, V_T and K_1 increased in all brain regions after tariquidar administration, displaying a similar pattern per brain region in baseline and after-inhibition scans. The K_1 was the parameter most affected by P-gp inhibition. In 91-min scan duration, the whole-brain region K_1 increased by 40.7% from 0.19 ± 0.01 at baseline to 0.26 ± 0.01 in after-inhibition scans, whereas the V_T increased from 10.6 ± 0.5 to 13.8 ± 0.1, an increase of 30.4%.

In two of the three subjects, the k_2 values remained similar in baseline and in after-inhibition scans, whereas one subject showed an increase in the k_2 values after the P-gp inhibition. However, the overall k_2 values did not significantly change after the treatment with tariquidar in any brain region. Figure 5 shows illustrative V_T, K_1, and k_2 parametric images at baseline and after-inhibition scans using 91-min scan.

V_T and K_1 increased significantly in all regions for all scan durations and subjects after the P-gp inhibition (see Tables S4−S7) while k_2 did not. Table 3 shows the K_1 and V_T values

https://dx.doi.org/10.1021/acs.molpharmaceut.0c00514
Mol. Pharmaceutics 2020, 17, 3477−3486

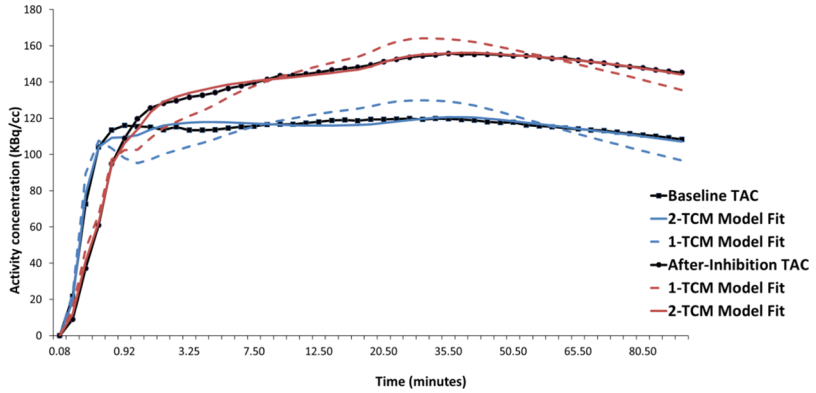

Figure 2. Representative 1-TCM (dashed line) and 2-TCM (solid line) fits of the whole brain at baseline (blue) and after-inhibition (red) scans, and the black circles and squares represent the baseline and after-inhibition TACs, respectively.

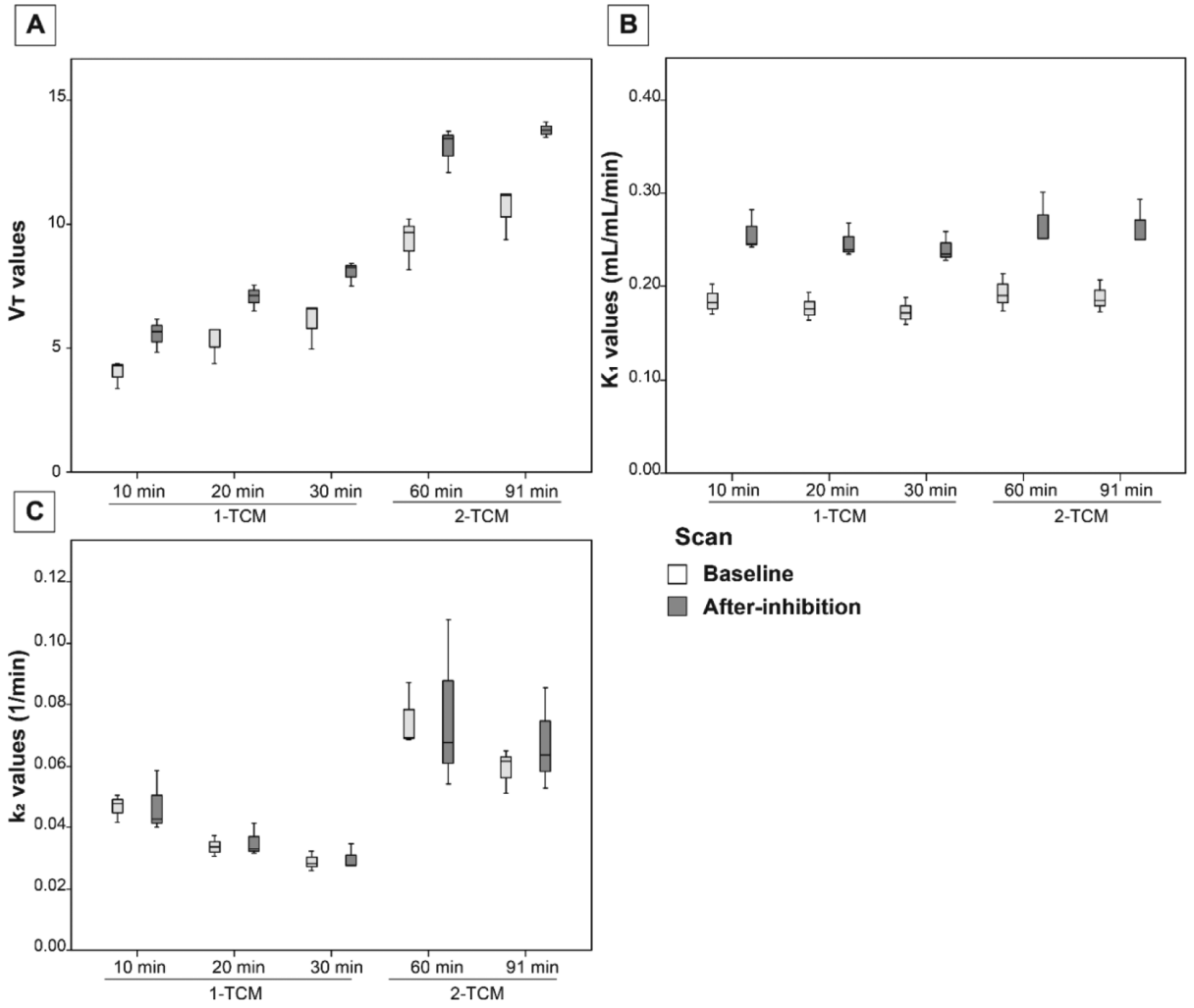

Figure 3. Boxplot showing the third quartile and first quartile range of K_1 (A), V_T (B), and k_2 (C) values of the whole-brain region at baseline and after-inhibition scans in different scan durations. The black line within the box marks the median and the whisker above and below the box indicates the maximum and the minimum value excluding the outliers.

at baseline and after-inhibition as well as the relative change (%) because of P-gp inhibition in 30 min scan duration.

4. DISCUSSION

The P-gp function at the BBB can be altered by different factors and could affect the distribution of several drugs inside the brain.[1,8,17,36,37] PET tracers, such as [^{18}F]MC225, may allow monitoring P-gp function and may identify potential DDIs.[13,38−40] This study investigated the suitability of [^{18}F]MC225 as a tracer for measuring P-gp function at the BBB of NHP. The study also explored the use of different methods for quantification of the P-gp function and various PET scan durations.

https://dx.doi.org/10.1021/acs.molpharmaceut.0c00514
Mol. Pharmaceutics 2020, 17, 3477−3486

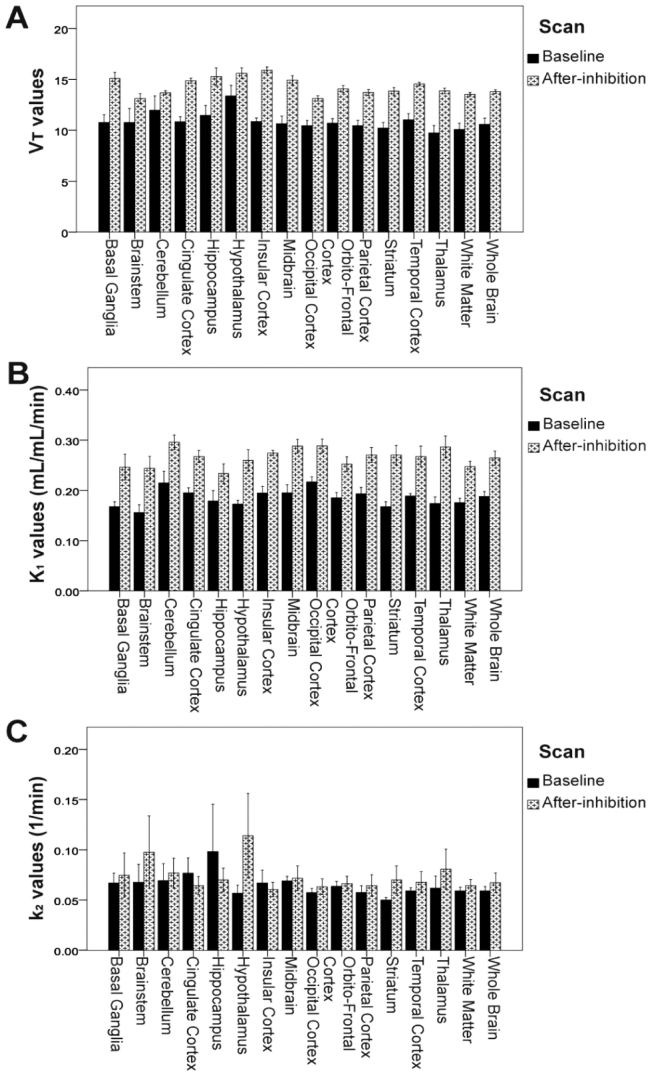

Figure 4. Mean ± SE of V_T (A), K_1 (mL/mL/min) (B) and k_2 (1/min) (C) for all the regions at baseline and after-inhibition scans using 91-min scan duration.

Blood analysis indicated that 50% of plasma radioactivity represented the parent tracer at 30 min after tracer injection. This differs from plasma pharmacokinetics in rats, where only 24% of the parent [^{18}F]MC225 was still available at that time-point.[15] This species difference can be expected because the rate of metabolism is smaller in bigger animals. The biological plasma $T_{1/2}$ remained similar after P-gp inhibition, suggesting that tracer elimination from the plasma was not significantly affected by the tariquidar intervention.

According to AIC and SE %, the most appropriate fit was found when v_B was fixed to 6% or used as a free-fit parameter (free v_B). Because restricting v_B did not improve the quality of the fits and robustness of the pharmacokinetic parameters, it was decided to use v_B as a free-fit parameter.

Next, we evaluated the preferred model for each scan duration. Lower AIC values for 2-TCM than for 1-TCM were observed for all studied scan durations. However, SE % V_T with 2-TCM was extremely large for short scan durations and in some cases higher than 1000%. Therefore, we preferred the use of 1-TCM for the analysis of short scans (<30 min) and the use of 2-TCM for long scans (60 and 91 min). The previous validation of [^{18}F]MC225 in rats had also shown unrealistically high V_T for 2-TCM because of very large SE % of K_1-k_4. Therefore, 1-TCM was selected as the preferred kinetic model for [^{18}F]MC225 in rats.[15]

In line with the above discussed previous study, our results showed that the estimation of V_T and k_2 is sensitive to scan duration while K_1 is not.[15] For baseline scans, the whole brain V_T increased by 165%, from 4 for the 10 min to 10.6 for the 91-min data. The k_2 also varied inconsistently with scan duration. This behavior is caused by the need to use different kinetic models for short (1-TCM) and long scan durations (2-TCM).

Inhibition of P-gp by a tariquidar challenge increased K_1 and V_T significantly in all the scan durations. These changes were smaller compared with those seen in rats, where the whole brain K_1 was 575% and the V_T 159% higher in tariquidar-treated rats than in control rats.[15] For baseline scans, rat's values were similar to NHP (K_1 (mL/mL/min) NHP = 0.19 vs K_1 rats = 0.12; V_T NHP = 9.33 vs V_T rats = 7.7). However, after P-gp inhibition, the values in rats were higher than the ones in NHP (K_1 NHP = 0.27 vs K_1 rats = 0.81; V_T NHP = 13.08 vs V_T rats = 20).[15] These differences may be explained by the dose of tariquidar used in these experiments. Rats were injected i.v. 30 min before the PET scan with a dose of 8 mg/kg, which is considered the maximum effective dose in rodents, whereas the NHPs were injected with a dose of 8 mg/kg at 15

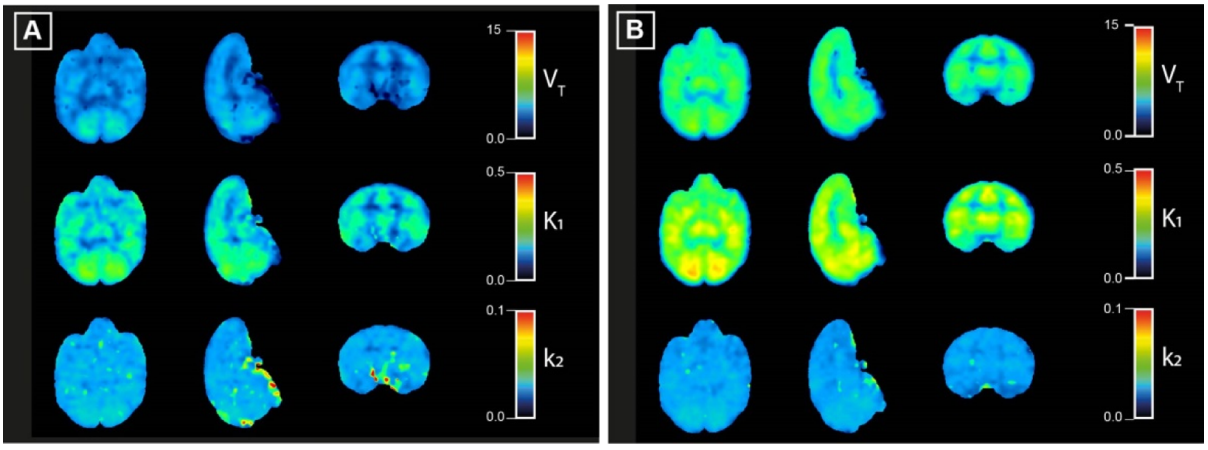

Figure 5. Parametric images calculated using 91-min scan duration and 2-TCM at baseline (A) and after-inhibition (B).

https://dx.doi.org/10.1021/acs.molpharmaceut.0c00514
Mol. Pharmaceutics 2020, 17, 3477−3486

Table 3. EMM ± SE of V_T and K_1 at Baseline and after-Inhibition in 30 min Scan Duration for All the Regions and p Values of the Difference between Baseline and after-Inhibition Scans

scan duration 30 min				
region	V_T baseline ± SE	V_T after-inhibition ± SE	% change V_T	p value
basal ganglia	5.5 ± 0.4	7.9 ± 0.2	45	$p < 0.001$
brainstem	5.5 ± 0.7	6.4 ± 0.3	15.9	$p = 0.321$
cerebellum	7.5 ± 0.9	8.3 ± 0.3	11	$p = 0.419$
cingulate cortex	6.4 ± 0.5	8.7 ± 0.2	36.5	$p < 0.001$
orbito-frontal cortex	5.8 ± 0.3	8 ± 0.3	36	$p = 0.001$
hippocampus	6 ± 0.6	7.5 ± 0.3	24.1	$p < 0.001$
hypothalamus	5.7 ± 0.4	7.4 ± 0.3	29.5	$p = 0.013$
insular cortex	6 ± 0.1	9.2 ± 0.4	54.1	$p < 0.001$
midbrain	5.9 ± 0.4	8.7 ± 0.2	46.3	$p < 0.001$
occipital cortex	6.4 ± 0.4	8.4 ± 0.2	30.4	$p < 0.001$
parietal cortex	6.1 ± 0.3	8.5 ± 0.3	39.5	$p < 0.001$
striatum	5.5 ± 0.4	8.2 ± 0.2	48.1	$p < 0.001$
temporal cortex	6.2 ± 0.5	8.2 ± 0.3	31.8	$p = 0.003$
thalamus	5.7 ± 0.4	8.2 ± 0.3	45.9	$p < 0.001$
white matter	5.6 ± 0.4	7.7 ± 0.2	37.3	$p < 0.001$
whole brain	6 ± 0.4	8 ± 0.2	33	$p = 0.001$
scan duration 30 min				
region	K_1 baseline ± SE	K_1 after-inhibition ± SE	% change K_1	p value
basal ganglia	0.15 ± 0.01	0.22 ± 0.01	44.9	$p < 0.001$
brainstem	0.14 ± 0.01	0.21 ± 0.01	49	$p < 0.001$
cerebellum	0.19 ± 0.01	0.27 ± 0.01	36.8	$p < 0.001$
cingulate cortex	0.17 ± 0.01	0.24 ± 0.01	40.1	$p < 0.001$
orbito-frontal cortex	0.17 ± 0.01	0.23 ± 0.01	36.1	$p < 0.001$
hippocampus	0.16 ± 0.01	0.21 ± 0.01	34.6	$p < 0.001$
hypothalamus	0.16 ± 0.01	0.22 ± 0.01	36.6	$p < 0.001$
insular cortex	0.18 ± 0.01	0.25 ± 0.01	43.9	$p < 0.001$
midbrain	0.18 ± 0.01	0.26 ± 0.01	47.8	$p < 0.001$
occipital cortex	0.2 ± 0.01	0.27 ± 0.01	32.1	$p < 0.001$
parietal cortex	0.18 ± 0.01	0.25 ± 0.01	39	$p < 0.001$
striatum	0.16 ± 0.01	0.24 ± 0.01	55.3	$p < 0.001$
temporal cortex	0.17 ± 0	0.24 ± 0.01	39.6	$p < 0.001$
thalamus	0.16 ± 0.01	0.26 ± 0.01	60.6	$p < 0.001$
white matter	0.16 ± 0.01	0.23 ± 0.01	39.4	$p < 0.001$

min before the PET scan.[15,16] In order to reach complete P-gp inhibition in NHP, a higher dose would have been required. Another possibility is that a longer period of time between the tariquidar injection and the PET scan is required to observe a larger P-gp inhibition effect in NHPs.

Taking into account all brain regions, the changes in K_1 between baseline and after-inhibition remained similar for all scan durations tested (42−44%) while the change in V_T varied from 40% using 10 min data to 32% in 91-min scan data. Moreover, K_1 changes caused by the P-gp inhibition were larger than those seen with V_T.

The previous pharmacokinetic evaluation of [^{18}F]MC225 in rats also showed that inhibition with tariquidar caused larger changes in K_1 (6−11-fold increase compared with baseline) than in V_T (2−4-fold increase).[15] This previous publication and our NHP study support the use of K_1 as a suitable parameter to measure the P-gp function at the BBB.[20,21] Because K_1 can be affected by changes in blood flow, we recommend the performance of an additional PET study (e.g. using [^{15}O]H_2O) for measuring the blood flow in order to assess the P-gp function more precisely.[20,21]

However, if changes in the blood flow occurred because of the treatment with tariquidar, the k_2 values would have also increased in the after-inhibition scans because this parameter also possesses information about flow, tracer extraction, and partition coefficient.[41] The results of our study did not find any significant increases in the k_2 values after the administration of tariquidar in any of the tested scan durations. It may be argued that the increase in k_2 values because of the blood flow effect may be masked because of the accumulation of radio metabolites, which may decrease the k_2. However, in short scan duration (10, 20 and 30 min), where the interference of the radio metabolites is negligible, the k_2 values did not change in after-inhibition scans in comparison to baseline values. Additionally, it has been published that the administration of the P-gp inhibitor cyclosporine-A caused changes in the K_1 of [^{11}C]verapamil tracer that cannot be explained by changes in the blood flow. The changes in blood flow, assessed using [^{15}O]H_2O scans, were smaller than the changes observed in the K_1 of [^{11}C]verapamil, thus these changes in K_1 may be mainly caused by the P-gp inhibition.[20]

Nevertheless, another approach to measure the P-gp function is to use other flow independent kinetic parameters, such as the V_T. Even though V_T estimations did not become stable at longer scan durations up to 60 min, SE % V_T decreased for scan durations longer than 60 min. Thus, V_T values estimated at scan durations greater than 60 min are more reliable than V_T values estimated from data of shorter

https://dx.doi.org/10.1021/acs.molpharmaceut.0c00514
Mol. Pharmaceutics 2020, 17, 3477−3486

scans. Moreover, because P-gp inhibition increased the whole-brain V_T by 40% (for 60 min scans) and by 30% (for 91 min scans), V_T obtained with 2-TCM may be used as a surrogate parameter to measure the P-gp function but requiring scans longer than 60 min. On the other hand, V_T obtained with long scan durations may be affected by the accumulation of radio metabolites inside the brain or by unspecific trapping of the tracer, and therefore, these values should be interpreted with caution. The latter may also explain the continued rise of V_T estimations in all tested scan durations.

Recent publications using another weak P-gp tracer, [^{11}C]metoclopramide, concluded that the most sensitive parameter to measure P-gp inhibition in NHP is V_T. After the infusion of tariquidar for 2 h at a dose of 4 mg/kg/h, V_T increased 2.2-fold compared to baseline. Despite the differences in dose of tariquidar and route of administration, the investigators observed an increase of 31% of K_1 after-inhibition, which is similar to the increase observed in our study. This study also found a significant decrease (1.64-fold) in the efflux rate constant k_2 after P-gp inhibition. The authors suggested that [^{11}C]metoclopramide may be used to measure altered transporter-mediated efflux reflected in changes of k_2.[42] However, our analysis did not find significant differences in k_2 between baseline and after-inhibition scans. A previous preclinical study performed with [^{18}F]MC225 found an increase in whole-brain k_2 values in rats previously exposed to isoflurane anesthesia compared to control rats. This increase in k_2 caused a decrease in V_T of the tracer inside the brain, however, it did not correspond to an increase in P-gp brain expression as was confirmed with western blot studies.[43] Therefore, if [^{18}F]MC225 is used to measure P-gp function at the BBB, the K_1 may be considered as the best parameter to assess the target function. Future studies such as a head to head comparison of both tracers are needed to clarify the mechanism of action of [^{11}C]metoclopramide and [^{18}F]MC225 and evaluate their sensitivity and specificity for measuring the P-gp transporter function.

In addition, recently the toxicity effects of MC225 were evaluated in male and female Sprague Dawley rats. The results of this study indicated that MC225 at a dose of 2.5 mg/kg body weight, which is the 10,000−fold equivalent of the postulated maximum administration dose (0.25 μg/kg body weight), did not cause toxicity to the animals during the following 14 days of observation. Moreover, the *Salmonella typhimurium* and *Escherichia coli* mutation test did not reveal any mutagenic activity.[44] Although the toxicity of MC225 was not evaluated in NHP, these positive results may set the stage for the clinical evaluation of [^{18}F]MC225.

5. CONCLUSIONS

This study investigates the use of different kinetic models to assess P-gp function as a function of varying scan durations. For short scan durations, the preferred model to quantify [^{18}F]MC225 PET in NHP is the 1-TCM, and the most suitable parameter to estimate the P-gp function is K_1. For long scan durations (>60 min), 2-TCM is the preferred model, and in this case, both K_1 and V_T can be used to estimate P-gp function at the BBB. Overall, our results suggest that the P-gp function at the BBB can be measured using either K_1 obtained by applying 1-TCM to 10 min of scan data or using K_1 and V_T obtained with 2-TCM for 91-min scan duration. These conclusions are in line with previous studies performed in rats and mice and warrant further studies in humans to confirm the properties of [^{18}F]MC225.

■ ASSOCIATED CONTENT

Supporting Information

The Supporting Information is available free of charge at https://pubs.acs.org/doi/10.1021/acs.molpharmaceut.0c00514.

Scan data, PET/MRI, reference MRI, and tissue probability maps, EMM ± SE of AIC, SE % K_1, and SE % V_T for all the brain regions at different scan durations at baseline and after-inhibition scans using different models, mean ± SE of V_T and SE % V_T for all the brain regions in short PET scans using 2-TCM, EMM ± SE of V_T at baseline and after-inhibition scans in short scan durations for all the regions and p values of the difference between baseline and after-inhibition scans, EMM ± SE of V_T at baseline and after-inhibition scans in long scan durations for all the regions and p values of the difference between baseline and after-inhibition scans, EMM ± SE of K_1 at baseline and after-inhibition in short scan durations for all the regions and p values of the difference between baseline and after-inhibition scans, and EMM ± SE of K_1 at baseline and after-inhibition scans in long scan durations for all the regions and p values of the difference between baseline and after-inhibition scans (PDF)

■ AUTHOR INFORMATION

Corresponding Author

Gert Luurtsema − *Department of Nuclear Medicine and Molecular Imaging, University of Groningen, University Medical Center Groningen, Groningen 9713 GZ, the Netherlands*; Email: g.luurtsema@umcg.nl

Authors

Lara García-Varela − *Department of Nuclear Medicine and Molecular Imaging, University of Groningen, University Medical Center Groningen, Groningen 9713 GZ, the Netherlands*; orcid.org/0000-0001-9803-4708

Wejdan M. Arif − *Department of Nuclear Medicine and Molecular Imaging, University of Groningen, University Medical Center Groningen, Groningen 9713 GZ, the Netherlands; Department of Radiological Sciences, College of Applied Medical Sciences, King Saud University, Riyadh, Saudi Arabia*

David Vállez García − *Department of Nuclear Medicine and Molecular Imaging, University of Groningen, University Medical Center Groningen, Groningen 9713 GZ, the Netherlands*

Takeharu Kakiuchi − *Central Research Laboratory, Hamamatsu Photonics KK, Hamamatsu, Shizuoka 434-8601, Japan*

Hiroyuki Ohba − *Central Research Laboratory, Hamamatsu Photonics KK, Hamamatsu, Shizuoka 434-8601, Japan*

Norihiro Harada − *Central Research Laboratory, Hamamatsu Photonics KK, Hamamatsu, Shizuoka 434-8601, Japan*

Tetsuro Tago − *Research Team for Neuroimaging, Tokyo Metropolitan Institute of Gerontology, Tokyo 173-0015, Japan*

Philip H. Elsinga − *Department of Nuclear Medicine and Molecular Imaging, University of Groningen, University Medical Center Groningen, Groningen 9713 GZ, the Netherlands*

Hideo Tsukada − *Central Research Laboratory, Hamamatsu Photonics KK, Hamamatsu, Shizuoka 434-8601, Japan*

https://dx.doi.org/10.1021/acs.molpharmaceut.0c00514
Mol. Pharmaceutics 2020, 17, 3477−3486

Nicola Antonio Colabufo − *Department of Pharmacy, University of Bari Aldo Moro, Bari 70121, Italy; Biofordrug, Spin-off Università degli Studi di Bari "A. Moro", Bari 70019, Italy;* orcid.org/0000-0001-5639-7746
Rudi A. J. O. Dierckx − *Department of Nuclear Medicine and Molecular Imaging, University of Groningen, University Medical Center Groningen, Groningen 9713 GZ, the Netherlands*
Aren van Waarde − *Department of Nuclear Medicine and Molecular Imaging, University of Groningen, University Medical Center Groningen, Groningen 9713 GZ, the Netherlands*
Jun Toyohara − *Research Team for Neuroimaging, Tokyo Metropolitan Institute of Gerontology, Tokyo 173-0015, Japan*
Ronald Boellaard − *Department of Nuclear Medicine and Molecular Imaging, University of Groningen, University Medical Center Groningen, Groningen 9713 GZ, the Netherlands*

Complete contact information is available at: https://pubs.acs.org/10.1021/acs.molpharmaceut.0c00514

Notes

The authors declare no competing financial interest.

REFERENCES

(1) Löscher, W.; Potschka, H. Role of Drug Efflux Transporters in the Brain for Drug Disposition and Treatment of Brain Diseases. *Prog. Neurobiol.* **2005**, *76*, 22−76.
(2) Ballabh, P.; Braun, A.; Nedergaard, M. The Blood-Brain Barrier: An Overview: Structure, Regulation, and Clinical Implications. *Neurobiol. Dis.* **2004**, *16*, 1−13.
(3) Van Asperen, J.; Mayer, U.; Van Tellingen, O.; Beijnen, J. H. The Functional Role of P-Glycoprotein in the Blood−Brain Barrier. *J. Pharm. Sci.* **1997**, *86*, 881−884.
(4) Abbott, N. J.; Patabendige, A. A. K.; Dolman, D. E. M.; Yusof, S. R.; Begley, D. J. Structure and Function of the Blood-Brain Barrier. *Neurobiol. Dis.* **2010**, *37*, 13−25.
(5) Engelhardt, B. Development of the Blood-Brain Barrier. *Cell Tissue Res.* **2003**, *314*, 119−129.
(6) Gameiro, M.; Silva, R.; Rocha-Pereira, C.; Carmo, H.; Carvalho, F.; Bastos, M. D. L.; Remião, F. Cellular Models and In Vitro Assays for the Screening of Modulators of P-Gp, MRP1 and BCRP. *Molecules* **2017**, *22*, 600.
(7) Zhou, S.-F. Structure, Function and Regulation of P-Glycoprotein and Its Clinical Relevance in Drug Disposition. *Xenobiotica* **2008**, *38*, 802−832.
(8) Silva, R.; Vilas-Boas, V.; Carmo, H.; Dinis-Oliveira, R. J.; Carvalho, F.; de Lourdes Bastos, M.; Remião, F. Modulation of P-Glycoprotein Efflux Pump: Induction and Activation as a Therapeutic Strategy. *Pharmacol. Ther.* **2015**, *149*, 1−123.
(9) Hartz, A. M. S.; Pekcec, A.; Soldner, E. L. B.; Zhong, Y.; Schlichtiger, J.; Bauer, B. P-Gp Protein Expression and Transport Activity in Rodent Seizure Models and Human Epilepsy. *Mol. Pharm.* **2017**, *14*, 999−1011.
(10) Vogelgesang, S.; Warzok, R.; Cascorbi, I.; Kunert-Keil, C.; Schroeder, E.; Kroemer, H.; Siegmund, W.; Walker, L.; Pahnke, J. The Role of P-glycoprotein in Cerebral Amyloid Angiopathy; Implications for the Early Pathogenesis of Alzheimers Disease. *Curr. Alzheimer Res.* **2004**, *1*, 121−125.
(11) Droździk, M.; Białecka, M.; Myśliwiec, K.; Honczarenko, K.; Stankiewicz, J.; Sych, Z. Polymorphism in the P-Glycoprotein Drug Transporter MDR1 Gene: A Possible Link between Environmental and Genetic Factors in Parkinson's Disease. *Pharmacogenetics* **2003**, *13*, 259−263.
(12) Kortekaas, R.; Leenders, K. L.; van Oostrom, J. C. H.; Vaalburg, W.; Bart, J.; Willemsen, A. T. M.; Hendrikse, N. H. Blood-Brain Barrier Dysfunction in Parkinsonian Midbrain in Vivo. *Ann. Neurol.* **2005**, *57*, 176−179.
(13) Luurtsema, G.; Elsinga, P.; Dierckx, R.; Boellaard, R.; Waarde, A. PET Tracers for Imaging of ABC Transporters at the Blood-Brain Barrier: Principles and Strategies. *Curr. Pharm. Des.* **2016**, *22*, 5779−5785.
(14) Savolainen, H.; Cantore, M.; Colabufo, N. A.; Elsinga, P. H.; Windhorst, A. D.; Luurtsema, G. Synthesis and Preclinical Evaluation of Three Novel Fluorine-18 Labeled Radiopharmaceuticals for P-Glycoprotein PET Imaging at the Blood-Brain Barrier. *Mol. Pharm.* **2015**, *12*, 2265−2275.
(15) Savolainen, H.; Windhorst, A. D.; Elsinga, P. H.; Cantore, M.; Colabufo, N. A.; Willemsen, A. T.; Luurtsema, G. Evaluation of [18F]MC225 as a PET radiotracer for measuring P-glycoprotein function at the blood-brain barrier in rats: Kinetics, metabolism, and selectivity. *J. Cereb. Blood Flow Metab.* **2017**, *37*, 1286−1298.
(16) Kuntner, C.; Bankstahl, J. P.; Bankstahl, M.; Stanek, J.; Wanek, T.; Stundner, G.; Karch, R.; Brauner, R.; Meier, M.; Ding, X.; et al. Dose-Response Assessment of Tariquidar and Elacridar and Regional Quantification of P-Glycoprotein Inhibition at the Rat Blood-Brain Barrier Using (R)-[11C]Verapamil PET. *Eur. J. Nucl. Med. Mol. Imaging* **2010**, *37*, 942−953.
(17) Feldmann, M.; Koepp, M. ABC Transporters and Drug Resistance in Patients with Epilepsy. *Curr. Pharm. Des.* **2016**, *22*, 5793−5807.
(18) Pereira, C. D.; Martins, F.; Wiltfang, J.; da Cruz e Silva, O. A. B.; Rebelo, S. ABC Transporters Are Key Players in Alzheimer's Disease. *J. Alzheimer's Dis.* **2017**, *61*, 463−485.
(19) Wang, W.; Bodles-Brakhop, A. M.; Barger, S. W. A Role for P-Glycoprotein in Clearance of Alzheimer Amyloid?-Peptide from the Brain. *Curr. Alzheimer Res.* **2016**, *13*, 615−620.
(20) Muzi, M.; Mankoff, D. A.; Link, J. M.; Shoner, S.; Collier, A. C.; Sasongko, L.; Unadkat, J. D. Imaging of Cyclosporine Inhibition of P-Glycoprotein Activity Using 11C-Verapamil in the Brain: Studies of Healthy Humans. *J. Nucl. Med.* **2009**, *50*, 1267−1275.
(21) Lubberink, M. Kinetic Models for Measuring P-Glycoprotein Function at the Blood-Brain Barrier with Positron Emission Tomography. *Curr. Pharm. Des.* **2016**, *22*, 5786−5792.
(22) Renkin, E. M. Transport of Potassium-42 from Blood to Tissue in Isolated Mammalian Skeletal Muscles. *Am. J. Physiol.-Legacy Content* **1959**, *197*, 1205−1210.
(23) Crone, C. The Permeability of Capillaries in Various Organs as Determined by Use of the 'Indicator Diffusion' Method. *Acta Physiol. Scand.* **1963**, *58*, 292−305.
(24) Morris, E. D.; Endres, C. J.; Schmidt, K. C.; Christian, B. T.; Muzic, R. F.; Fisher, R. E. Kinetic Modeling in Positron Emission Tomography. *Emission Tomography*; Elsevier, 2004; Vol. *46*, pp 499−540.
(25) Uchida, Y.; Wakayama, K.; Ohtsuki, S.; Chiba, M.; Ohe, T.; Ishii, Y.; Terasaki, T. Blood-Brain Barrier Pharmacoproteomics-Based Reconstruction of the In Vivo Brain Distribution of P-Glycoprotein Substrates in Cynomolgus Monkeys. *J. Pharmacol. Exp. Ther.* **2014**, *350*, 578−588.
(26) Bauer, M.; Karch, R.; Zeitlinger, M.; Philippe, C.; Römermann, K.; Stanek, J.; Maier-Salamon, A.; Wadsak, W.; Jäger, W.; Hacker, M.; et al. Approaching Complete Inhibition of P-Glycoprotein at the Human Blood-Brain Barrier: An (R)-[11C]Verapamil PET Study. *J. Cereb. Blood Flow Metab.* **2015**, *35*, 743−746.
(27) Bauer, M.; Karch, R.; Neumann, F.; Wagner, C. C.; Kletter, K.; Müller, M.; Löscher, W.; Zeitlinger, M.; Langer, O. Assessment of Regional Differences in Tariquidar-Induced P-Glycoprotein Modulation at the Human Blood-Brain Barrier. *J. Cereb. Blood Flow Metab.* **2010**, *30*, 510−515.
(28) Müllauer, J.; Karch, R.; Bankstahl, J. P.; Bankstahl, M.; Stanek, J.; Wanek, T.; Mairinger, S.; Müller, M.; Löscher, W.; Langer, O.; et al. Assessment of Cerebral P-Glycoprotein Expression and Function with PET by Combined [11C]Inhibitor and [11C]Substrate Scans in Rats. *Nucl. Med. Biol.* **2013**, *40*, 755−763.
(29) Gunn, R. N.; Summerfield, S. G.; Salinas, C. A.; Read, K. D.; Guo, Q.; Searle, G. E.; Parker, C. A.; Jeffrey, P.; Laruelle, M. Combining PET Biodistribution and Equilibrium Dialysis Assays to

Assess the Free Brain Concentration and BBB Transport of CNS Drugs. *J. Cereb. Blood Flow Metab.* **2012**, *32*, 874−883.
(30) Fan, J.; de Lannoy, I. A. M. Pharmacokinetics. *Biochem. Pharmacol.* **2014**, *87*, 93−120.
(31) Frey, S.; Pandya, D. N.; Chakravarty, M. M.; Bailey, L.; Petrides, M.; Collins, D. L. An MRI Based Average Macaque Monkey Stereotaxic Atlas and Space (MNI Monkey Space). *Neuroimage* **2011**, *55*, 1435−1442.
(32) Calabrese, E.; Badea, A.; Coe, C. L.; Lubach, G. R.; Shi, Y.; Styner, M. A.; Johnson, G. A. A Diffusion Tensor MRI Atlas of the Postmortem Rhesus Macaque Brain. *Neuroimage* **2015**, *117*, 408−416.
(33) McLaren, D. G.; Kosmatka, K. J.; Oakes, T. R.; Kroenke, C. D.; Kohama, S. G.; Matochik, J. A.; Ingram, D. K.; Johnson, S. C. A Population-Average MRI-Based Atlas Collection of the Rhesus Macaque. *Neuroimage* **2009**, *45*, 52−59.
(34) Ashburner, J. A fast diffeomorphic image registration algorithm. *Neuroimage* **2007**, *38*, 95−113.
(35) Andersen, P. K. 1. Generalized Estimating Equations. James W. Hardin and Joseph M. Hilbe, Chapman and Hall/CRC, Boca Raton, 2003. No. of Pages: Xiii+ 222 Pp. Price:$79.95. ISBN 1-58488-307-3. *Stat. Med.* **2004**, *23*, 2479−2480.
(36) Assema, D.; Berckel, B. Blood-Brain Barrier ABC-Transporter P-Glycoprotein in Alzheimer's Disease: Still a Suspect? *Curr. Pharm. Des.* **2016**, *22*, 5808−5816.
(37) Gottesman, M. M.; Ambudkar, S. V. Overview: ABC Transporters and Human Disease. *J. Bioenerg. Biomembr.* **2001**, *33*, 453−458.
(38) Kannan, P.; John, C.; Zoghbi, S. S.; Halldin, C.; Gottesman, M. M.; Innis, R. B.; Hall, M. D. Imaging the Function of P-Glycoprotein With Radiotracers: Pharmacokinetics and In Vivo Applications. *Clin. Pharmacol. Ther.* **2009**, *86*, 368−377.
(39) Toyohara, J. Importance of P-Gp PET Imaging in Pharmacology. *Curr. Pharm. Des.* **2016**, *22*, 5830−5836.
(40) Tournier, N.; Stieger, B.; Langer, O. Imaging Techniques to Study Drug Transporter Function in Vivo. *Pharmacol. Ther.* **2018**, *189*, 104−122.
(41) Carson, R. E. Tracer Kinetic Modeling in PET. *Positron Emission Tomography*; Springer-Verlag: London, 2003; pp 127−159.
(42) Auvity, S.; Caillé, F.; Marie, S.; Wimberley, C.; Bauer, M.; Langer, O.; Buvat, I.; Goutal, S.; Tournier, N. P-Glycoprotein (ABCB1) Inhibits the Influx and Increases the Efflux of 11 C-Metoclopramide across the Blood-Brain Barrier: A PET Study on Non-Human Primates. *J. Nucl. Med.* **2018**, *118*, 1609−1615.
(43) García-Varela, L.; Vállez García, D.; Rodríguez-Pérez, M.; van Waarde, A.; Sijbesma, J. W. A.; Schildt, A.; Kwizera, C.; Aguiar, P.; Sobrino, T.; Dierckx, R. A. J. O.; et al. Test-Retest Repeatability of [18F]MC225-PET in Rodents: A Tracer for Imaging of P-gp Function. *ACS Chem. Neurosci.* **2020**, *11*, 648−658.
(44) Toyohara, J.; Sakata, M.; Tago, T.; Colabufo, N. A.; Luurtsema, G. Automated Synthesis, Preclinical Toxicity, and Radiation Dosimetry of [18F]MC225 for Clinical Use: A Tracer for Measuring P-Glycoprotein Function at the Blood-Brain Barrier. *EJNMMI Res.* **2020**, *10*, 84.

https://dx.doi.org/10.1021/acs.molpharmaceut.0c00514
Mol. Pharmaceutics 2020, 17, 3477−3486